ELSEVIER

Cement & Concrete Composites 26 (2004) 275–290

Cement & Concrete Composites

www.elsevier.com/locate/cemconcomp

Flexural strength predictions of steel fiber reinforced high-strength concrete in fully/partially prestressed beam specimens

S.K. Padmarajaiah [a], Ananth Ramaswamy [b,*]

[a] Department of Civil Engineering, IIT Roorkee, UP, India

[b] Department of Civil Engineering, Indian Institute of Science, Bangalore 560012, India

Received 28 November 2001; accepted 15 October 2002

Abstract

This study presents results from an experimental program for eight fully prestressed beams and seven partially prestressed beams made with high strength fiber-reinforced concrete (plain concrete strength of 65 MPa). These studies mainly attempted to determine the influence of trough-shaped steel fibers in altering the flexural strength at first crack and ultimate, the load–deflection and moment–curvature characteristics, ductility and energy absorption capacity of the beams. The magnitude of the prestress, volume fraction of the fibers ranging from 0% to 1.5% and the location of fibers were the variables in the test program.

Analytical models to determine the load–deflection and moment–curvature relationships as a function of the fiber volume fraction have been formulated. Empirical relationships for the ultimate strength, first crack load level, load versus deflection and moment versus curvature as a function of fiber content have been proposed by making use of force equilibrium and compatibility considerations.

A primary finding emerging from the experimental program was that the placement of fibers over a partial depth in the tensile side of the prestressed flexural structural members provided equivalent flexural capacity as in a beam having the same amount of fiber over the full cross-section. In large scale precast concrete applications it is expected that this would be economical and lead to considerable cost saving in the design without sacrificing on the desired structural performance. The analytical models proposed in this study predicts the test results closely.

Keywords: Flexural strength; Partial depth fibers; Load–deflection response; Moment–curvature relationship; Fully/partially prestressed beams; High-strength fiber concrete; Analytical models

1. Introduction

High-strength concrete (HSC) has permitted the development of significantly larger span bridges and high-rise structures. But HSC has been found to be more brittle compared to normal strength concrete (NSC). This weakness is due to the inability of the materials to prevent small cracks, which can originate at a flaw or void in the material, from becoming unstable under small tensile stresses. The deficiencies of low tensile strength and insufficient ductility may be minimized by providing conventional steel in the tensile regions of the member to sustain the tensile stresses or by means of applying a precompression on the concrete cross-section, to alter the stress distribution. Inclusion of fibers in the concrete is another way of reducing the brittleness of HSC.

Addition of fibers has been shown to increase the flexural strength, and ductility of structures made of NSC with conventional reinforcement. But few such research studies have been undertaken to examine the role of fibers in the area of prestressed concrete applications. This aspect is very important in applications where the serviceability in terms of limits on the deflection and crack width controls the design.

Only a few studies have been reported in the literature, that have used the concept of inclusion of fibers over a partial depth of the beam in the area of NSC without tensile steel [2,14,16]. Swamy et al. [21] have

* Corresponding author. Fax: +91-80-3600-404.
E-mail address: ananth@civil.iisc.ernet.in (A. Ramaswamy).

0958-9465/$ - see front matter © 2002 Elsevier Ltd. All rights reserved.
doi:10.1016/S0958-9465(02)00121-X

Nomenclature

A_{ps} area of prestressing wire
A_s cross-sectional area of deformed bar
A_f cross-sectional area of fiber
C total force in the compressive stress block
D overall depth of the beam
d effective depth
d_p effective depth to prestressing wire
d_s effective depth to deformed bar
E_c, E_m initial tangent modulus of plain concrete
E_f modulus of elasticity of fiber
E_{fc} initial tangent modulus of fiber-reinforced concrete
E_p modulus of elasticity of prestressing wire
E_s Young's modulus of the deformed bar
F_{be} bond efficiency factor
f'_c and ϵ_c stress and strain values on the compressive stress–strain curve
f'_{cf} compressive strength of fiber-reinforced concrete
f_{ck} cube compressive strength of plain concrete
f''_{ck} cube strength of plain concrete at transfer of prestress
f_{ckf} cube compressive strength of fiber-reinforced concrete
f_t ultimate uniaxial tensile strength of plain concrete
f_{spcf} split cylinder strength SFRC
$f_{7,spcf}$ split cylinder strength of SFRC at the age of seven days
f_p characteristic strength of the prestressing wire
f_{pe} effective prestress
f_{py} yield strength of prestress wire
f_{pu} ultimate strength of prestress wire
f_{puy} difference between ultimate stress and yield stress of prestress wire
f_{sy} yield strength of deformed bar
f_{uy} ultimate strength of deformed bar
f_{suy} difference between ultimate stress and yield stress of deformed bar
l_c critical length of fiber
l_f/d_f fiber aspect ratio
M ultimate moment of resistance
M_c moment of resistance due to compressive force in concrete
M_{fl} flexural moment strength
M_{T1} moment of resistance of prestress force
M_{T2}, M_{T3} and M_{T4} moment due to tensile side of stress block developed in fiber-reinforced concrete
M_{T5} moment of tensile force due to deformed bar about the neutral axis
M-1, M-2 load predicted using model 1 and 2
r_f radius of fibers
s_f spacing of fibers
s_1 ratio of proportional limit to yield stress of prestress wire
s_2 ratio of the difference between the yield stress and proportional limit of prestress wire to the yield stress of prestressing wire
s_{11} ratio of proportional limit to yield stress of deformed bar
s_{22} ratio of the difference between the yield stress and proportional limit of deformed bar to the yield stress of deformed bar
T_1, T_5 tensile forces due to prestressing wire and deformed bar, respectively
T_2, T_3, T_4 tensile force due to fiber concrete
W applied load
x neutral axis depth
α flexural tensile stress coefficient
α^1 random fiber orientation factor
β material parameter for SFRC
δ deflection at center
δ_1 deflection at first crack
δ_2 deflection at 80% or 90% of the peak load beyond the peak load
ϵ_{0f} peak compressive strain of SFRC
ϵ_{fp} fiber strain at proportional limit
ϵ_{ce} concrete strain at the level of prestressing wire
ϵ_{cu} extreme compressive strain at ultimate
ϵ_m matrix tensile strain at peak tensile stress
ϵ_{0m} peak compressive strain of plain concrete
ϵ_p strain in prestressing wire due to loads
ϵ_{pb} total strain in prestressing wire
ϵ_{pe} effective strain in prestress wire
ϵ'_{puy} difference between ultimate strain and yield strain in prestress wire
ϵ_{puy} ultimate strain in prestress wire
ϵ_{py} yield strain in prestress wire
ϵ_{uy} ultimate strain in deformed bar
ϵ_s strain in deformed bar
ϵ_{sy} yield strain in deformed bar
ϵ_{suy} difference between ultimate strain and yield strain in deformed bar
η_b bond efficiency factor
η_o fiber orientation factor
η_l length correction factor
μ partial depth factor
ϕ curvature

σ_f	force carried by fibers per unit area	σ_{tt}	effective tensile stress in the fiber-reinforced concrete
σ_c	uniaxial compressive strength of plain concrete	τ_d	ultimate bond stress between fiber and concrete
σ_m, σ_{mu}	tensile strength of matrix		

studied the behavior of concrete beams with conventional reinforcements and having fibers placed over a partial depth of the section.

Analytical models proposed by various researchers for determining the flexural strength of NSC without tensile reinforcement [1,3,7,20] and SFRC with conventional reinforcement [4,5,15,21] were based on an assumed stress block, and were validated using their respective test results. The stress–strain response of HSC elements is different from that of NSC and hence alternate models need to be developed to predict the ultimate flexural strength of fiber-reinforced HSC elements. The principal concern in analytical studies on the flexural behavior of steel fiber reinforced prestressed concrete has been the prediction of the ultimate flexural strength of the structure in terms of various material parameters. Insufficient attention has been given to the deformational behavior. This aspect is important in applications where serviceability in terms of deflections is a consideration.

Thus the major emphasis of the present study has been to determine using experimental studies the basic mechanical properties of HSC elements containing fibers and thus experimentally assess the structural behavior of prestressed HSC beams containing fibers. Development of analytical models to predict the flexural behavior of high strength FRC prestressed beam in terms of first crack load, peak loads, crack width, load–deflection, and moment–curvature characteristics when the fibers were distributed over full depth or partial depth and over full span or only in the shear span in the tensile side of the beams, was another objective of the present work.

2. Experimental program

2.1. Materials

The main constituents used to cast all the 15 fully and partially prestressed beams were ordinary Portland cement conforming to IS: 269 [8], natural river sand (uncrushed) passing through IS sieve no. 7 (2.36 mm) and conforming to IS:383 [9], coarse aggregate (12.5 mm and smaller) conforming to IS:383 [9] zone II classification, water, superplasticizer (brand name Conplast-430) 1.2 wt.% of cement, and trough (similar to hooked end) shaped mild carbon steel fibers having an average length

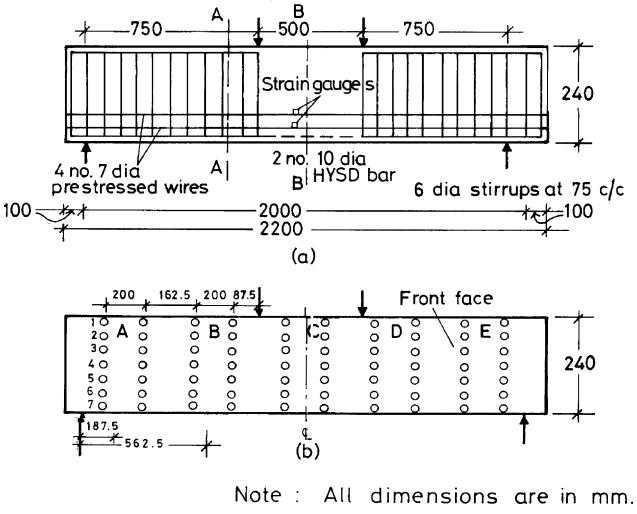

Fig. 1. (a). Experimental set-up and loading arrangements for flexure critical prestressed beam specimens and (b) details of Demac point locations.

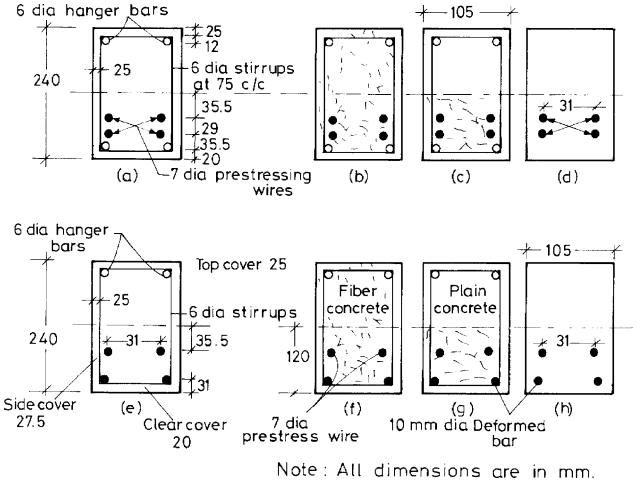

Fig. 2. (a) Cross-sectional details for fully prestressed plain concrete specimen A-FP/f0-0; (b) cross-sectional details for full depth fiber-reinforced prestressed concrete beam specimens A-FP/f0-5, A-FP/f1-0, and A-FP/f1-5; (c) cross-sectional details for fully prestressed beam specimens with half depth fiber A-FPhf/f1-0 and A-FPhf/f1-5 (c) and (d) cross-sectional details of for specimen A-FPhs/f1-0 and A-FPhs/f1-5 having partial depth fiber in shear span only; (e) cross-sectional details for partially prestressed plain concrete specimen A-PP/f0-0; (f) cross-sectional details for full depth fiber-reinforced concrete partially prestressed beam specimens A-PP/f0-5, A-PP/f1-0, and A-PP/f1-5; (g) cross-sectional details for half depth fiber-reinforced partially prestressed beam specimen A-PPhf/f1-0 and A-PPhf/f1-5 (g) and (h) cross-sectional details of partially prestressed beam specimen A-PPhs/f1-0 and A-PPhs/f1-5 having partial depth fiber in shear span only.

Table 1
Summary of results for fully and partially prestressed beams

Sl	Beam	v_f (%)	At transfer		At testing			At first crack (kN)			At peak (kN)		
			Age (days)	f''_{ck} (MPa)	Age (days)	f_{ckf} (MPa)	f_t (MPa)	Expt.	M-1	M-2	Expt	M-1	M-2
1	A-FP/f0-0	0	9	48.39	29	64.96	5.23	55.43	43.8	43.8	96.99	96.28[a]	96.28
2	A-FP/f0.5	0.5	9	48.39	29	65.62	5.93	59.94 (8.0)	48.30 (10.82)	48.54 (10.82)	104.21 (7.45)	110.50 (14.77)	107.77 (11.92)
3	A-FP/f1-0	1.0	7	50.36	29	66.71	8.62	60.00 (8.5)	53.29 (21.68)	53.29 (21.68)	112.40 (15.85)	117.63 (22.0)	109.21 (13.50)
4	A-FP/f1-5	1.5	7	50.36	29	68.02	10.13	64.46 (16.40)	58.05 (32.5)	58.05 (32.5)	117.314 (20.97)	119.13 (23.75)	111.53 (16.00)
5	A-FPhf/F1-0	1.0	11	54.35	29	66.71	8.21	58.14 (5.0)	53.29 (21.68)	53.29 (21.68)	106.92 (10.25)	117.33 (22)	110.45 (14.72)
6	A-FPhf/f1-5	1.5	11	54.35	29	67.36	10.03	64.46 (16.29)	58.05 (32.5)	58.05 (32.5)	110.54 (14.0)	118.99 (23.6)	111.81 (16.07)
7	A-FPhs/f1-0	1.0	11	54.35	29	66.71	8.21	56.87 (3)	43.80 (–)	43.80 (–)	99.24 (2)	96.28[a] (2.5)	96.28 (–)
8	A-FPhs/f1-5	1.5	11	54.35	29	67.36	10.03	57.95 (4.5)	43.80 (–)	43.80 (–)	101.47 (4.0)	96.28[a] (5.0)	96.28 (–)
9	A-PP/f0-0	0	6	47.09	30	65.18	5.31	42.780	26.30	26.30	91.66	83.8[a]	83.80
10	A-PP/f1-0	1.0	6	47.09	30	66.05	8.78	50.91 (18.18)	35.89 (36)	35.89 (36)	105.116 (14.73)	99.151 (18.32)	106.45 (27.03)
11	A-PP/f1-5	1.5	7	53.48	30	68.02	10.35	55.421 (28.67)	40.5 (54)	40.5 (542)	109.634 (19.66)	100.250 (19.6)	110.10 (31.30)
12	A-PPhf/f1-0	1.0	7	49.85	29	66.27	8.21	46.39 (15.37)	38.89 (48)	38.89 (48)	101.503 (10.8)	98.4 (17.42)	106.18 (26.71)
13	A-PPhf/f1-5	1.5	7	53.48	29	68.02	10.35	55.425 (28.67)	40.56 (54)	40.56 (54)	105.116 (14.73)	100.31 (19.7)	108.65 (29.65)
14	A-PPhs/f1-0	1.0	7	49.85	29	66.27	8.21	46.39 (7.71)	26.30	26.30	96.985 (5.9)	–	–
15	A-PPhs/f1-5	1.5	7	53.48	30	68.23	10.35	46.39 (7.71)	26.3	26.30	99.244 (8.32)	–	–

[a] Assumed same as model 2, values in the parenthesis are in % increase over plain concrete beams.

(l_f) of 40 mm, and a nominal diameter (d_f) of 0.5 mm. Prestressing wire (7 mm diameter), high-strength deformed bars (10 mm diameter) and mild steel reinforcing bars as shear stirrups (6 mm diameter) were used to cast the HSC prestressed beams. The fiber content used in this study was 0%, 0.5%, 1.0%, and 1.5% of the volume of concrete.

In this investigation, procedures reported in a standard code (IS Hand book SP:23 [19]) were adopted to determine the basic properties of the constituent materials. The design mix was arrived at by a process of trial and error. For an assumed water cement ratio (w/c) of 0.5 the trial mix design using the procedure outlined in IS Handbook SP:23 [19] and by Nagaraj and Banu [10] was arrived at and cubes were tested at 28 days to determine the compressive strength of the final mix proportion. The final design mix used to cast all the beams was 1:1.128:1.385 (cement:fine aggregate:coarse aggregate), with a w/c ratio of 0.36, in order to achieve a 28 day cube strength of 65 MPa for plain concrete.

2.2. Specimen details and testing procedure

Figs. 1 and 2 show the reinforcement and cross-sectional details of fully and partially prestressed beam specimens. The reinforcement cage consisted of mild steel stirrups of 6 mm diameter with 75 mm center to center spacing and were provided only in the shear span in order to ensure adequate shear capacity leading to a flexural failure. The middle portion of the beam (pure moment zone) had no shear reinforcement. Pretensioning of the high-tensile wires was done between the two anchor heads of the pretensioning bed, casting four beams at a time. Each wire of 7 mm diameter was tensioned using a 10 ton Killick Nixon hydraulic Jack by stressing one wire at a time up to a load of 3.6 ton. In the case of fully prestressed concrete members, four high-tensile wires were used. A cover of 20 mm for the prestress wires was used for the fully prestressed pretensioned beams (IS-1343) [23] while a 30 mm cover was used for the deformed bars in the partially prestressed beam specimen. In partially prestressed beams two high-tensile wires were used for prestressing. Electrical resistance strain gauges of 15 mm gauge length, having a resistance of 118–124 Ω and a gauge factor of 2.14, were used on both the prestressing wires and the deformed bar. The strain gauges were glued to the wires and suitably covered using insulation tape and bees wax before concreting. The prestressing force was transferred 6–11 days after the casting of concrete. Thereafter, the prestressed specimens were removed from the pretensioning bed and cured under wet jute bags for 28 days. Table 1 gives the material property details for each of the 15 specimens at transfer and at testing. In Fig. 2 and Table 1, the nomenclature A-FP/f1-0, implies fully prestressed (FP) beams having 1% fiber content (f1-0). The letters 'hf' in the specimen (e.g. A-FPhf/f1-5) implies half the depth fiber in the tensile side of the beam. The letter 'A' is common to the entire series of beams discussed in this paper. The letter 'hs' in the specimen (e.g. A-FPhs/f1-0) implies half the depth fibers only in the shear span, and the letter 'PP' implies partially prestressed beam specimen.

All the beams were tested at the age of 29 to 30 days after casting using a 500 kN capacity loading frame. The typical test set-up and Demec gauge locations on the concrete surface have been shown in Fig. 1(a) and (b). Fig. 2(a)–(h) show the cross-sectional details of the specimens tested in this study. The loading rollers were placed 750 mm from the support. The load was applied in increments of 4.5 kN till the development of the first visible microcracks. A careful visual inspection to observe the initiation of hairline cracks was made during the course of the test. The crack widths were measured in all the segments and at all levels of load (except the last stage of loading) using a microscope having a least count of 0.01 mm. The crack pattern and the crack growth at different stages of loading were marked on the specimen at each load level with a pencil line indicating the crack initiation and propagation at a particular load level during the course of the test. A load control procedure was adopted for the test program. After the peak load value, the deflections were recorded as the load was getting released gradually, indicating the softening beyond the peak. This approach was resorted to due to a lack of stroke control facility. As will be shown later, the analytical response under predicts the softening observed in the test. This may be attributed to the limitations in the test procedure used in this study. The results from the tests are shown in Table 1. The complete crack patterns were transferred to a graph sheet to get the spacing of cracks at different stages of loading upon completion of the test. The companion cube strength, split cylinder strength and modulus of rupture (using prisms) tests were carried out on the same day as the corresponding tests on the prestressed beams.

3. Analytical models

A simple refined analysis procedure has been developed in the present investigation for predicting the complete deformational behavior, viz., moment vs. curvature and load vs. deflection relationship, and load vs. steel strain, for the HSC prestressed beams containing fibers. The analytical procedures accounts for postcracking tensile resistance of concrete with fibers and improved ductility of trough-shaped steel fiber reinforced concrete under tensile and compressive stresses.

In this study two analytical models have been proposed accounting for the presence of fibers over either the full depth or half depth in the tensile side of the fully or partially prestressed beam cross-section (Fig. 3(a) and (f), Fig. 4(a) and (f)). Model 1 (Fig. 3(b) and (c)) is based on the modified stress block proposed by Swamy et al. [21] and Henager and Doherty [5]. As shown in Fig. 3(b) the model considers the compressive side stress block as a modified serpentine curve which has the same shape as the compressive stress–strain curve of high-strength steel FRC proposed in this research program and has been reported in [12] (shown as Eq. (1) for completeness). In model 1 the compressive stress–strain curve has been extended up to a depth equal to 'z' from the extreme compressive face (Fig. 3(b)), and the tensile side stress block is trapezoidal in shape. The peak tensile stress σ_m at a depth z from the extreme compression fiber, shown in Fig. 3(b) corresponds to the tensile stress σ_f (corresponding strain of ϵ_f shown in Fig. 3(c)) described later by Eq. (4). The corresponding extreme fiber tensile stress σ_{tt} is as described later by Eq. (6). The computation of the stress quantities using Eqs. (4) and (6), as discussed later, is very complex requiring several other material parameters not easily available. Model 2, shown in Fig. 3(d) and (e) has been newly developed in this study simplifying the formulation considerably in computing the tensile stress quantities σ_m and σ_{tt} of model 1 through the use of the plain concrete tensile strength and the split cylinder tensile strength of SFRC (shown later in Eq. (29)), respectively for these parameters. Only the cube compressive strength of concrete is needed to compute the stress parameters. The compression side of the stress block in model 2 has been assumed to be the same as used in model 1 and is extend up to the level of cracking strain in the matrix. Fig. 3(f)–(j) describe the application of model 1 and 2 for partially prestressed beams. Fig. 4(a)–(j) describe the application of model 1 and 2 for fully or partially prestressed beams having fibers over a partial depth of the cross-section (μD in Fig. 4).

In the flexural analysis procedure the complete moment–curvature relationship has been constructed by finding the values of moment corresponding to different input extreme fiber concrete compressive strain values. For each value of the compressive strain, through a process of trial and error, the neutral axis position which satisfies the equilibrium of the total compression carried by concrete and tensile forces carried by FRC, prestressing wires and reinforcement bar has been obtained. Knowing the neutral axis depth and extreme compressive strain, the curvature and stresses in the cross-section have been calculated. The process has been terminated with the commencement of concrete crushing.

The total strain in the prestressing wire is $(\epsilon_{pb}) = \epsilon_{ce} + \epsilon_{pe} + \epsilon_p$, where $\epsilon_{pe} = f_{pe}/E_p$ is the effective strain in

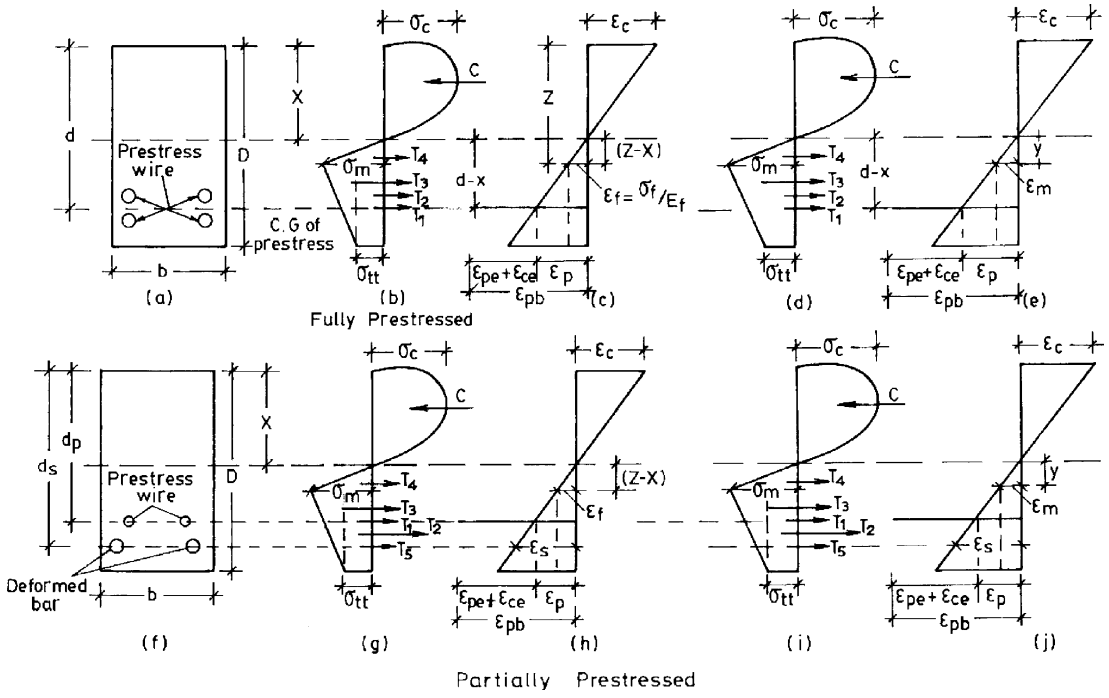

Fig. 3. (a) Cross-sectional details, (b) and (c) stress and strain diagram for model 1, (d) and (e) stress and strain diagram for model 2 for fully prestressed beams; (f) cross-sectional details for partially prestressed beams, (g) and (h) stress and strain diagram for model 1 (i) and (j) stress and strain diagram for model 2 for partially prestressed beams.

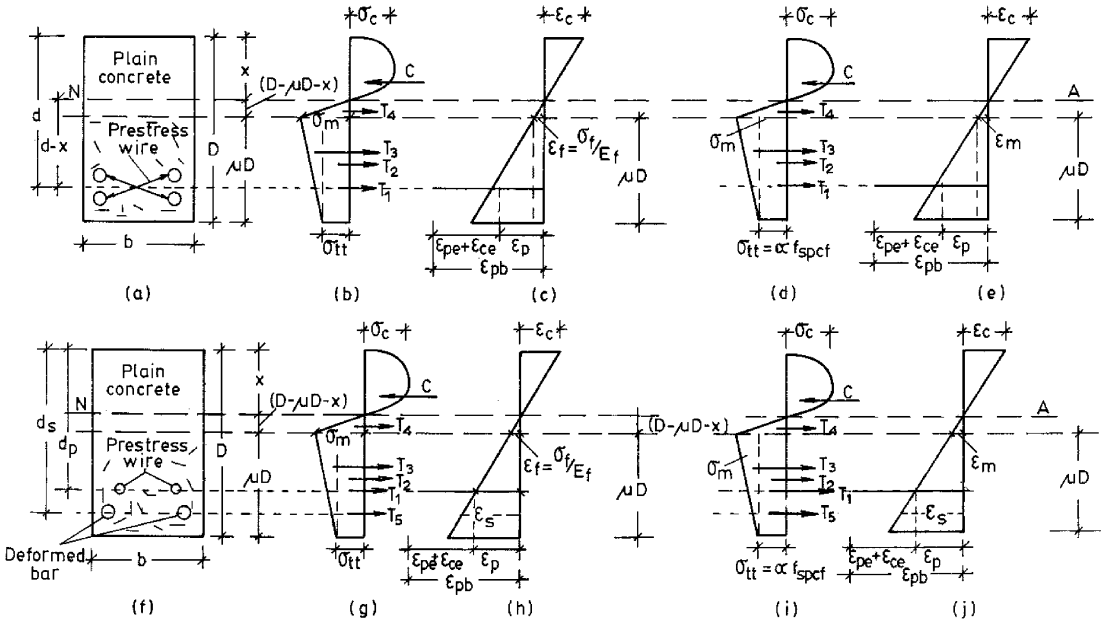

Fig. 4. (a) Cross-section for fully prestressed beam with partial depth fiber, (b) and (c) stress and strain variation diagram when the neutral axis lies in the plain reinforced-concrete zone in model 1, (d) and (e) stress and strain variation diagram when the neutral axis lies in the plain concrete zone in model 2, (f) cross-section for partially prestressed beam with partial depth fiber, (g) and (h) stress and strain variation diagram when the neutral axis lies in the plain reinforced-concrete zone in model 1, (i) and (j) stress and strain variation diagram when the neutral axis lies in the plain concrete zone in model 2.

the prestressing wire and ϵ_{ce} is the strain in concrete at the level of the prestressing wire that is transferred to the wire through bond. The stress–strain levels of the prestressing wire have been divided in to three portions viz., the proportional limit based on a limiting strain of 0.007 ($\epsilon_{pb} \leqslant 0.007$), a second portion up to yield strain (ϵ_{py}) of 0.011 (the corresponding stress (f_{py}) in the prestressing wire was 1551.45 MPa: $0.007 \leqslant \epsilon_{epb} \leqslant 0.011$) and a third portion up to an ultimate strain (ϵ_{pu}) was taken corresponding to an ultimate stress (f_{pu}) of 1598.5 MPa ($0.011 \leqslant \epsilon_{epb} \leqslant \epsilon_{puy}$) was taken. ϵ_{pb} is the total strain in the prestress wire at any stage, due to the effective prestress, strain in the surrounding concrete and the applied loads. Eq. (1) expressing the compressive stress–strain response which includes the descending component of the stress–strain response and the effect of trough-shaped fibers in concrete (fiber properties expressed in terms of reinforcement index, RI) is based on the results of a research program, the details of which have been presented by Padmarajaiah [11] and Padmarajaiah and Ramaswamy [12]. 'RI' is the fiber reinforcement index expressed in terms of the fiber volume fraction and aspect ratio ($v_f l_f/d_f$).

$$f'_c = f'_{cf}\left[\frac{\beta\left(\frac{\epsilon_c}{\epsilon_{0f}}\right)}{\beta - 1 + \left(\frac{\epsilon_c}{\epsilon_{0f}}\right)^{\beta}}\right]$$

$$\beta = 1.141488 + 0.5939(RI)^{-0.504528} \quad (1)$$

3.1. Fully prestressed sections

3.1.1. Full depth fiber-reinforced concrete beams: model 1

3.1.1.1. Case 1: When $\epsilon_{pb} \leqslant 0.007$. Fig. 3(b) and (c) shows the assumed stress distribution over the depth of the concrete section and the corresponding strain variation diagram. From the strain diagram (Fig. 3(c)):

$$\frac{\epsilon_c}{x} = \frac{\epsilon_p}{d - x} \quad (2)$$

The total strain in the prestressing wire is $(\epsilon_{pb}) = \epsilon_{ce} + \epsilon_{pe} + \epsilon_p$, where $\epsilon_{pe} = f_{pe}/E_p$ is the effective strain in the prestressing wire and ϵ_{ce} is the strain in concrete at the level of the prestressing wire transferred to the wire through bond. Also, from the strain diagram

$$z = x\frac{\epsilon_c + \epsilon_f}{\epsilon_c} \quad (3)$$

where the steel fiber strain $\epsilon_f = \sigma_f/E_f$. The value of σ_f is given by Henager and Doherty [5] and Henager [6] as:

$$\sigma_f = \frac{(2\tau_d F_{be} l_f)}{d_f} \quad (4)$$

τ_d is the bond stress between fiber and concrete. In the present study τ_d was evaluated from the modulus of rupture test data from the present research program [12] and chosen from the data table reported by

Swamy and Mangat [22] for straight fibers and is equal to τ_d of 2.44 MPa for the obtained modulus of rupture value. F_{be} is the bond efficiency factor equal to 1.0 for smooth, straight, round steel fibers given by Henager and Doherty [5] and Henager [6]. F_{be} depends on factors such as the water cement ratio, fiber type and shape, etc. The dependence of τ_d and F_{be} on fiber shape has been ignored due to paucity of data relating these parameters to the fiber shape and therefore the available information for straight fibers has been used in the present discussion. However, the model formulation retains the flexibility to incorporate these factors easily for situations where reliable data accounting for these factors is available.

From the stress diagram (Fig. 3(b)) the tensile stress intensity, σ_{tt}, is the effective tensile stress in the FRC. By assuming perfect bond between fibers and the matrix, the value of σ_{tt} is given by Swamy et al. [21] is:

$$\sigma_{tt} = 2\tau_d \mathrm{RI} \tag{5}$$

For Eq. (5) to be applicable to short-length fibers which are uniformly distributed, and randomly oriented, the expressions obtained by Swamy et al. [20] have been employed in the present study with some modifications. An orientation factor (η_o), due to the fact that a portion of the fibers will be inefficiently oriented has been included. Further a length correction factor (η_l) to account for the stress distribution at the end portion of the fibers of finite length has been considered. Finally, since the surface deformation of the fibers influences their bond with concrete, the bond efficiency factor (η_b) to account for the shape of the fibers, i.e., whether the fiber is straight, crimped, duoform, hooked, or trough shaped (used in the present study) has also been incorporated. Thus, Eq. (5), above has been modified as follows:

$$\sigma_{tt} = \eta_l \eta_o \eta_b 2\tau_d \mathrm{RI} \tag{6}$$

Comparing Eq. (4) and (6) it is seen that the effect of F_{be} has been decomposed and expressed in terms of the length, orientation and bond efficiency factors. A portion of the fibers will be uniformly distributed and randomly oriented with respect to the principal axis. In three-dimensional solids, in which fibers can be oriented in any direction with equal probability, an orientation factor (α^1) of 0.41–0.64 have been proposed by Romualdi and Mandel [17]. The values of α^1 used by various investigators [7,18,21] range from 0.41 to 0.82. The orientation factors of 0.645 which corresponds to two-dimensional random orientation has been used in this study (mean value of 3-D and 2-D fiber orientation data from test results reported by Soroushian and Lee [18]). No precise data has been reported for the bond efficiency factor η_b, and the values assigned by Henager [6], equal to 1.0 for straight fibers, has been used in the present study. The length orientation factor that accounts for the varying fiber stress at the end potion of the fibers, proposed by Swamy et al. [21], is given by:

$$\eta_l = 1 - \frac{\tan h(\beta_1 l_f/2)}{\beta_1 l_f/2} \tag{7}$$

where

$$\beta_1 = \sqrt{\frac{2\pi G_m}{E_f A_f \ln(s_f/r_f)}}$$

$G_m = E_c/2(1+v)$ is the matrix shear modulus, r_f is the radius of fibers, s_f is the spacing of fibers and is given by:

$$s_f = 25\left(\frac{d_f}{v_f l_f}\right)^{1/2}$$

where s_f is in mm and v_f is the fiber volume percentage. Thus, the equilibrium equation of forces acting on the cross-section is:

$$C = T_1 + T_2 + T_3 + T_4 \tag{8}$$

where C is the total force in the compressive stress block and is given by:

$$C = \int_0^x f'_c b\,\mathrm{d}x \tag{9}$$

The tensile force acting in the section is the summation of tensile force due to prestressing force T_1 and the tensile force due to FRC T_2, T_3, and T_4 (Fig. 3(b)).

$$T_1 = A_{ps} f_{pb} \tag{10}$$

$$T_2 = (D-z)\sigma_{tt} b \tag{11}$$

$$T_3 = 1/2(D-z)(\sigma_m - \sigma_{tt})b \tag{12}$$

$$T_4 = 1/2\sigma_m (z-x)b \tag{13}$$

Moment equilibrium equation is obtained by taking moment of all the above forces about the neutral axis

$$M = M_c + M_{T1} + M_{T2} + M_{T3} + M_{T4} \tag{14}$$

M_c = moment of resistance due to compressive force in concrete, i.e.:

$$M_c = C\bar{x} = \int_0^x (f'_c b\,\mathrm{d}x)x \tag{15}$$

M_{T1} is the moment of resistance due to prestressing force, and M_{T2}, M_{T3}, and M_{T4} are the moments of resistance mobilized by the stress block for the FRC on the tensile side, i.e.:

$$M_{T1} = T_1(d-x) \tag{16}$$

$$M_{T2} = T_2\left(\tfrac{1}{2}(D-z) + (z-x)\right) \tag{17}$$

$$M_{T3} = T_3\left(\tfrac{1}{3}(D-z) + (z-x)\right) \tag{18}$$

$$M_{T4} = T_4\tfrac{2}{3}(z-x) \tag{19}$$

3.1.1.2. Case 2: When the Strain in the prestressing wire ϵ_{pb} is in the region $0.007 \leqslant \epsilon_{pb} \leqslant 0.011$. The expression

representing the force in prestressing wire T_1 (Eq. (10)) is now given by:

$$T_1 = A_{ps}s_1 f_{py} + A_{ps}y_1 \tag{20}$$

$$y_1 = \frac{s_2 f_{py}(\epsilon_{pb} - 0.007)}{0.007} \tag{21}$$

The expressions for C, T_2, T_3, T_4 remain the same as before.

3.1.1.3. Case 3: When the strain ϵ_{pb} in the prestressing wire is in the region $0.011 \leqslant \epsilon_{epb} \leqslant \epsilon_{puy}$. The tensile force due to prestressing wire T_1 (Eq. (10)) is now given by:

$$T_1 = A_{ps}f_{py} + A_{ps}y_2 \tag{22}$$

where

$$y_2 = \frac{(\epsilon_{pb} - 0.011)}{\epsilon'_{puy}}(f_{puy})$$

3.1.2. Partial depth fiber-reinforced prestressed concrete beams

There are two situations which arise in the case of partial depth FRC beams depending upon the position of the neutral axis, viz., when the neutral axis lies in the FRC zone and when the neutral axis lies in the plain concrete zone. When the neutral axis lies within the concrete zone with fibers at a depth μd, the force equilibrium and moment equations remain the same as the equations derived in the previous section.

3.1.2.1. When the neutral axis lies in the plain concrete zone Case 1: When $\epsilon_{pb} \leqslant 0.007$. Referring to Fig. 4(a)–(c), the total compressive force 'C' due to concrete compression and tensile force due to prestressing wire are same as in the previous section (Eqs. (9) and (10)), but the other tensile force components due to concrete with fibers are as follows

$$T_2 = \sigma_{tt}\mu Db \tag{23}$$

$$T_3 = \tfrac{1}{2}(\sigma_m - \sigma_{tt})\mu Db \tag{24}$$

$$T_4 = \tfrac{1}{2}\sigma_m d(D - \mu D - x) \tag{25}$$

The moment equilibrium equations have been obtained by taking moment of all the forces about the neutral axis. Moment due to concrete in compression and moment due to prestressing force are the same as in the previous sections (Eqs. (15) and (16)). However, the moment contributions from the FRC tensile stress block about the neutral axis is given by:

$$M_{T2} = T_2\left[\left(\mu\frac{D}{2}\right) + (D - \mu D - x)\right] \tag{26}$$

$$M_{T3} = T_3\left[\left(\mu\frac{D}{3}\right) + (D - \mu D - x)\right] \tag{27}$$

$$M_{T4} = T_4\left[\frac{2}{3}(D - \mu D - x)\right] \tag{28}$$

3.1.3. Analysis of full depth fiber-reinforced concrete beams: model 2

The moment–curvature relationship developed in the present study using model 2 shown in Fig. 3(d) and (e), has been proposed based on the experimental work from the present study. Model 2 is simple compared to model 1, in that it requires only the cube strength of plain concrete for computing the extreme tensile stress σ_{tt}. This is in contrast to model 1, where the various fiber factors, viz., fiber orientation factor (η_o), fiber bond efficiency factor (η_b), length correction factor (η_l), and bond strength (τ_d) were the important quantities required to compute the extreme fiber tensile strength, σ_{tt}, to quantify the contribution of the effect of fibers dispersed in the concrete.

The compression side of the stress block for the model 2 is similar to model 1. But in the tensile side, it is assumed that at cracking, the modulus of rupture σ_m of plain concrete is the same as the tensile strength of concrete σ_t and the values of extreme tensile strength σ_{tt} is assumed as equal to αf_{spcf} for the tensile block as shown in Fig. 3. The value of α was 0.833 and f_{spcf} is the split cylinder tensile strength of FRC (Eq. (29)) proposed in the present research program, details of which are reported in [11,12].

$$f_{spcf} = \sqrt{f_{ck}}/3 + 1.918(\mathrm{RI}) \tag{29}$$

3.1.3.1. Case 1: When $\epsilon_{pb} \leqslant 0.007$. The force and moment equilibrium equations developed in this sections are similar to model 1 except, that the value of the extreme tensile strength of the tensile block σ_{tt} becomes αf_{spcf}.

From the strain diagram (Fig. 3(e)),

$$y = \frac{\epsilon_m}{\epsilon_p}(d_p - x) \tag{30}$$

$$\epsilon_m = \frac{\sigma_m}{E_c} \tag{31}$$

The compressive force in concrete and the tensile force due to prestressing wires are the same as in Eqs. (9) and (10). The tensile force due to fiber-reinforced concrete is computed, referring to Fig. 3(d) as:

$$T_2 = (D - x - y)\sigma_{tt}b \tag{32}$$

$$T_3 = \tfrac{1}{2}(D - x - y)(\sigma_m - \sigma_{tt})b \tag{33}$$

$$T_4 = \tfrac{1}{2}\sigma_m y b \tag{34}$$

The moment contribution from the different forces about neutral axis is:

$$M_{T2} = T_2\left[\frac{(D-x-y)}{2}+y\right] \tag{35}$$

$$M_{T3} = T_3\left[\frac{(D-x-y)}{3}+y\right] \tag{36}$$

$$M_{T4} = T_4\left[\frac{2}{3}y\right] \tag{37}$$

The case where $\epsilon_{pb} > 0.007$ and $\leqslant 0.011$ and $\epsilon_{pb} < \epsilon_{puy}$ are similar to the discussions in the proceeding sections for model 1.

3.2. Partially prestressed fiber-reinforced concrete beams

The stress–strain response levels for the deformed bar have been divided into three zones. The modulus of elasticity for the steel has been taken as 197.5 GPa. Yield stress (457.8 MPa) has been taken at a strain level of 0.004. The proportional limit has been taken at a strain level of 0.002 and ultimate strain has been taken at the corresponding ultimate strength (534.76 MPa) of the deformed bar. The equilibrium equation can be obtained for the three cases viz., (1) when the strain in the deformed bar (ϵ_s) is $\leqslant 0.002$; (2) when the strain in the deformed bar satisfies $0.002 \leqslant \epsilon_s \leqslant 0.004$; and (3) when the strain in the deformed bar $0.004 \leqslant \epsilon_s \leqslant \epsilon_{uy}$. Models 1 and 2 are similar to that employed in the fully prestressed beam studied, except that the strain in the deformed bar has been employed to demarcate the different stress–strain regions (Fig. 3(f)–(j)).

3.2.1. Full depth fiber-reinforced concrete beams: model 1
3.2.1.1. Case 1: When $\epsilon_s \leqslant 0.002$. The equilibrium equation for the forces in the section is:

$$C = T_1 + T_2 + T_3 + T_4 + T_5 \tag{38}$$

The force equilibrium equations and moment expressions due to T_1, T_2, T_3, and T_4 are the same as for the fully prestressed beams. The tensile force due to deformed steel bar T_5 and the corresponding moment about the neutral axis are:

$$T_5 = A_s f_y \tag{39}$$

$$M_{T5} = T_5(d_s - x) \tag{40}$$

3.2.1.2. Case 2: When the strain in the deformed bar $0.002 \leqslant \epsilon_s \leqslant 0.004$. The expressions representing the force in deformed steel T_5, is now given by

$$T_5 = A_s s_{11} f_{sy} + A_s y_1' \tag{41}$$

From the stress–strain curve of the deformed bar,

$$y_1' = \frac{s_{22} f_{sy}(\epsilon_s - 0.002)}{0.002}$$

The prestressing wire remains in the elastic linear region under this condition.

3.2.1.3. Case 3: Deformed bar: $0.004 \leqslant \epsilon_s \leqslant e_{uy}$, prestressing wire: $0.007 \leqslant \epsilon_{pb} \leqslant 0.011$, and $0.011 \leqslant \epsilon_{pb} \leqslant e_{puy}$. In this strain level range, the tensile force due to deformed bar is given by

$$T_5 = A_s f_{sy} + A_s y_2' \tag{42}$$

where

$$y_2' = (\epsilon_s - 0.004)\frac{f_{suy}}{\epsilon_{suy}}$$

The magnitude of stresses in prestressing wires have been computed in the same way as reported earlier for the different strain levels. Similar to fully prestressed beams, in partially prestressed beams having partial depth of fibers, two situations arises depending upon the position of neutral axis, namely, when the neutral axis lies in fiber zone and when the neutral axis lies in plain concrete zone. The force equilibrium equations obtained for each situation is similar to those obtained for the fully prestressed beams reported earlier.

4. Results and discussion

Material properties of concrete and steel and the experimental and analytical results for all the beams studied have been reported in Table 1. Figs. 5 and 6 show the load–deflection diagram for fully and partially prestressed beam specimens having fiber content of v_f 0%, 0.5%, 1.0%, and 1.5%, respectively. From the load–deflection curve (Figs. 5 and 6) and Table 1 it is clearly seen that, both cracking load and ultimate flexural load increased as the fiber content increased. The peak load was found to be 104.216 kN, 112.40 kN, and 117.31 kN for the beams A-FP/f0-5, A-FP/f1-0, and A-FP/f1-5, respectively. In the partially prestressed beams A-PP/f0-0, A-PP/f1-0, and A-PP/f1-5 the ultimate peak load was

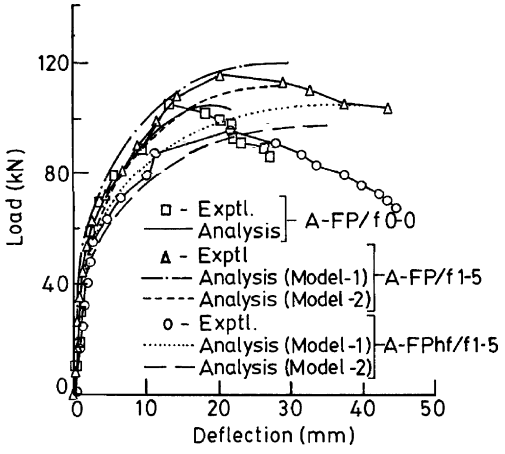

Fig. 5. Load verses deflection response for fully prestressed beam specimens.

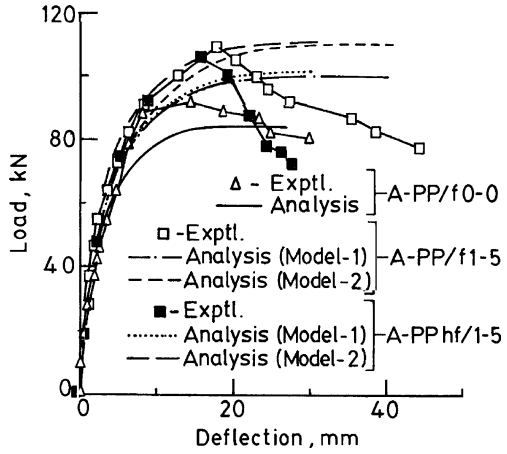

Fig. 6. Load verses deflection response for partially prestressed beam specimens.

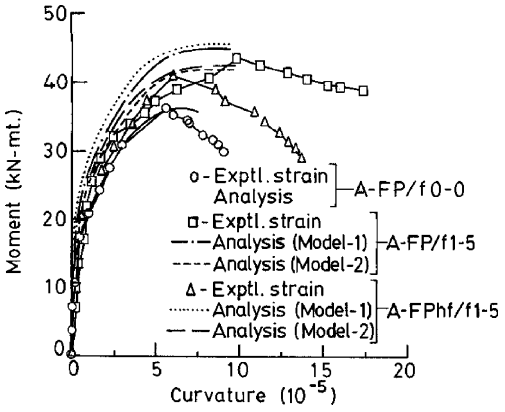

Fig. 7. Moment verses curvature response for fully prestressed beam specimens.

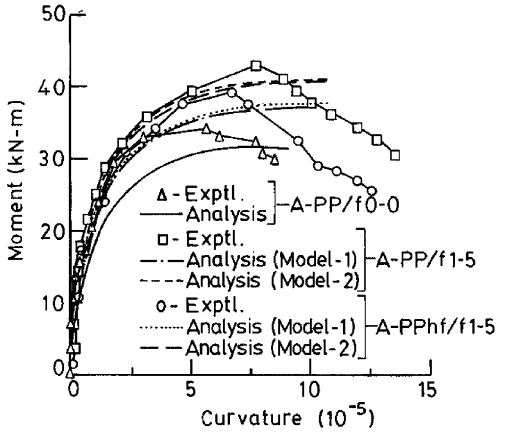

Fig. 8. Moment verses curvature response for partially prestressed beam specimens.

found to be 91.66 kN, 105.12 kN, and 109.63 kN, respectively. It can also be seen from the load–deflection response, that as the fiber content increased, at a particular load level the deflection was found to be reduced.

From the examination of Table 1 and Figs. 5 and 6, it seen that, in both fully/partially prestressed beams, there is quantitatively no significant difference in the behavior of beams with partial depth fiber compared to the behavior of the corresponding beams with full depth fiber. It is seen that inclusion of fibers, only in half the depth on the tensile side, is effective in bringing about the improvements in the deformational characteristics to almost at par with those obtained with full depth fiber beams, from the initial loading stage up to the ultimate load. However, full depth fiber inclusion imparts increased ductility and preserves the structural integrity of the members up to the ultimate stage. Table 1 also shows the load details for the fully prestressed beams (A-FPhs/f1-0 and A-FPhs/f1-5) and partially prestressed beams (A-PPhs/f1-0 and A-PPhs/f1-5), where the fibers were in half depth only in the shear span. From Table 1 it is seen that, the cracking load values for these beams were almost the same as in plain concrete beams. As the cracks developed in the flexure region due to increase in loads, the contribution of fibers in the flexure region declined and, no fibers came in to play to enhance the flexure strength.

The inclusion of fibers in the fully prestressed beams resulted in higher ultimate strengths as compared to the corresponding partially prestressed beams. Further in partially prestressed beams, all the beams exhibited lower cracking loads compared to the corresponding fully prestressed beams. Greater deflection was observed under loads in partially prestressed beams. In the case of partially prestressed beams failure was due to yielding of deformed steel and spalling of concrete on the compressive side.

From Figs. 7 and 8, which show the moment vs. curvature response for the tested beams, it is seen that full depth and partial depth fiber-reinforced prestressed concrete beam specimens have practically the same modifying effect on the deformational characteristics, viz., curvature of the beams at all the stages of loading. The curvatures were considerably reduced, thereby increasing the stiffness of the prestressed beams from the beginning up to failure. A larger fiber content has a greater influence in modifying these characteristics. Full depth fiber inclusion is more advantages in improving the ductility characteristics at failure. The moment–curvature response for the case of beams having partial depth SFRC only in the shear span (beams A-FPhs/f1-0, A-FPhs/f1-5 in Fig. 7; A-PPhs/f1-0, A-PPhs/f1-5 in Fig. 8) shows that there is no difference in the curvature diagram due to addition of fiber when compared to the plain concrete beam response.

Tables 2 and 3 show the comparison of analytically predicted loads, deformational characteristics, and

Table 2
Comparison of analytical results at various stages of loading for fully prestressed beam specimens

Beam	Stages	Expt.			Analysis: model 1			Analysis: model 2		
		W (kN)	δ (mm)	ϕ (10^{-3})	W (kN)	δ (mm)	ϕ (10^{-3})	W (kN)	δ (mm)	ϕ (10^{-3})
A-FP/0-0										
	1	19.40	0.59	0.09	–	–	–	19.26	0.50	0.09
	Ratio				–	–	–	0.99	0.85	1.00
	2	55.43	2.68	1.08	–	–	–	43.80	1.65	0.81
	Ratio				–	–	–	0.79	0.62	0.75
	3	64.66	4.47	1.71	–	–	–	64.20	4.48	1.66
	Ratio				–	–	–	1.01	1.00	0.97
	4	96.99	13.50	5.62	–	–	–	96.28	18.40	6.22
	Ratio				–	–	–	0.99	1.36	1.11
A-FP/f1-5										
	1	21.40	0.56	0.18	23.42	0.51	0.19	2.09	0.51	0.20
	Ratio				1.09	0.91	0.95	1.03	0.91	1.11
	2	58.14	2.20	0.81	53.30	1.61	0.41	53.30	1.65	0.53
	Ratio				0.92	0.73	0.51	0.92	0.75	0.66
	3	71.28	3.52	1.98	78.21	4.57	1.38	73.63	4.30	1.43
	Ratio				1.10	1.29	0.70	1.03	1.22	0.72
	4	106.92	16.56	6.28	117.33	24.54	7.14	110.45	21.25	7.2
	Ratio				0.91	1.48	1.14	1.03	1.28	1.15
A-FPhf/f1-5										
	1	22.11	0.59	0.18	24.24	0.61	0.19	22.40	0.61	0.19
	Ratio				1.09	1.03	1.06	1.01	1.03	1.06
	2	64.46	2.11	0.80	58.05	1.98	0.61	58.05	1.99	0.65
	Ratio				0.90	0.94	0.76	0.90	0.94	0.81
	3	73.69	3.71	1.93	80.80	4.25	1.29	74.54	4.33	1.57
	Ratio				1.09	1.15	0.70	1.01	1.16	0.81
	4	110.54	17.50	6.16	118.99	27.40	7.76	111.81	26.10	8.82
	Ratio				1.09	1.56	1.25	1.01	1.49	1.43
A-FPhs/f1-5										
	1	20.29	0.62	0.20	–	–	–	19.26	0.50	0.09
	Ratio				–	–	–	0.95	0.81	0.45
	2	57.95	2.58	0.70	–	–	–	43.80	1.65	0.81
	Ratio				–	–	–	0.76	0.64	1.16
	3	67.65	4.01	1.25	–	–	–	64.20	4.48	1.66
	Ratio				–	–	–	0.95	1.12	1.32
	4	101.47	16.10	5.23	–	–	–	96.28	18.40	6.22
	Ratio				–	–	–	0.95	1.14	1.99

moment–curvature response at four different stages of loading, viz., before crack initiation, at first flexure crack, at working load (peak load/1.5) and at peak load level. A comparison of the analytically obtained load–deflection curve and the moment–curvature response with test results, shown in Figs. 5–8 and Tables 2 and 3, reveals that the proposed model is in good agreement with the test results at all the stages of loading. In the precracked elastic stage 1 in Tables 2 and 3, the ratios (analytical to experimental values) of the load, deflection and curvature range from 0.9 to 1.0. At working load levels (peak load/1.5) the model predictions are quite accurate (ratios of analytical to experimental load, deflection and curvature values for each beam at stage 3 vary between 0.85 and 1.04) and is a useful tool for practicing engineers planning to specify the use of full or partial depth fibers in design. Due to addition of fibers both models predicted an increased flexural strength observed in the test results. In the postpeak region full depth fiber inclusion improves to a considerable extent extreme concrete compressive strains, steel strains, ultimate curvatures and central deflections. From Tables 2 and 3, it is seen that, the analytical predictions of the ultimate flexural strength and various deformational characteristics increased with the addition of fibers as compared to plain concrete beams. The analytical predictions are close to experimental results over the full range of the load deformational response. The ratio of flexural strength of analytically computed results to experiment results was found to be in the ranges of 0.9–1.01 at all the four stages of loading. As indicated earlier, the analytical model under predicts the degree of softening beyond the peak load. This may be attributed to the load control method adopted in the test

Table 3
Comparison of analytical results at various stages of loading for partially prestressed beam specimens

Beam	Stages	Expt.			Analysis: model 1			Analysis: model 2		
		W (kN)	δ (mm)	ϕ (10^{-3})	W (kN)	δ (mm)	ϕ (10^{-3})	W (kN)	δ (mm)	ϕ (10^{-3})
A-PP/0-0										
	1	18.33	0.54	0.04	–	–	–	16.76	0.50	0.08
	Ratio				–	–	–	0.91	0.93	2.00
	2	42.78	2.33	0.41	–	–	–	26.30	1.15	0.32
	Ratio				–	–	–	0.62	0.50	0.78
	3	61.10	4.10	1.18	–	–	–	55.87	3.74	1.21
	Ratio				–	–	–	0.91	0.91	1.03
	4	91.65	14.30	5.68	–	–	–	83.80	17.50	6.21
	Ratio				–	–	–	0.91	1.22	1.11
A-PP/f1-5										
	1	21.93	0.65	0.18	20.05	0.60	0.20	22.02	0.60	0.20
	Ratio				0.91	0.92	1.11	1.00	0.92	1.11
	2	55.43	2.40	0.77	40.50	1.65	0.58	40.50	1.65	0.58
	Ratio				0.73	0.69	0.76	0.73	0.69	0.76
	3	73.09	4.85	1.39	66.83	4.50	1.43	73.40	4.50	1.43
	Ratio				0.91	0.93	1.03	1.00	0.93	1.03
	4	109.63	17.98	7.77	100.25	28.16	9.98	110.10	28.16	9.98
	Ratio				0.91	1.56	1.28	1.00	1.56	1.28
A-PPhf/f1-5										
	1	21.02	0.63	0.29	20.06	0.61	0.27	21.73	0.63	0.21
	Ratio				0.95	0.97	0.93	1.03	1.00	0.73
	2	55.43	2.13	0.88	40.56	1.67	0.56	40.56	1.67	0.47
	Ratio				0.74	0.78	0.64	0.73	0.80	0.54
	3	70.08	4.70	1.62	66.87	4.40	2.01	72.43	4.00	1.59
	Ratio				0.95	0.94	1.24	1.04	0.85	0.98
	4	105.12	16.00	6.75	100.31	28.01	8.03	108.65	21.25	8.21
	Ratio				0.95	1.75	1.19	1.03	1.33	1.21
A-PPhs/f1-5										
	1	19.85	0.85	0.21	–	–	–	16.76	0.50	0.08
	Ratio				–	–	–	0.84	0.59	0.40
	2	46.39	1.9	0.54	–	–	–	26.30	1.15	0.32
	Ratio				–	–	–	0.60	0.61	0.60
	3	66.16	4.83	1.65	–	–	–	55.87	3.74	1.21
	Ratio				–	–	–	0.84	0.78	0.73
	4	99.24	20.89	8.72	–	–	–	83.80	17.50	6.21
	Ratio				–	–	–	0.84	0.84	0.71

procedure resulting in higher measurement levels of softening beyond the peak. However, in the peak region in both fully and partially prestressed beams model 2 predictions were better than the predictions based on model 1. Details of the crack pattern, spacing and width obtained in the tested beams along with procedures evolved to predict the crack spacing and width in this research program have been reported in [11,13].

4.1. Ductility and energy absorbed

In the present study, the ductility factor was obtained from the load–deflection diagram, by dividing the deflection δ_2 at 90% of the peak load, beyond the peak, to the deflection at first crack δ_1 (Fig. 5). The postpeak deflection level (at 90% of postpeak load level) was selected based on the availability of the deflections up to this level. In the case of partially prestressed beam specimens, it was possible to measure the deflection value in the test specimen e.g., A-PP/f0-0 (Fig. 6), corresponding to 80% of the peak load value beyond the peak. Hence, in the case of partially prestressed beam specimens, the ductility factor was determined by dividing the deflection at 80% of the ultimate load, beyond peak δ_2, to deflection at the first crack δ_1. The values of δ_1 and δ_2 have been tabulated in Table 4. Table 4 shows the ductility factor calculated for all 15 fully/partially prestressed beam specimens. It is seen that, load decreases after peak strength gradually and the total energy absorbed, in debonding and stretching of the fibers, before complete separation of the beam was higher for FRC prestressed beams than for plain concrete prestressed beam.

Table 4
Details of ductility factor (DF) and energy absorbed for fully and partially prestressed beam specimens

Sl	Beam	RI	δ_1 (mm)	δ_2 (mm)	DF = δ_2/δ_1	Incr. of DF (%)	Energy (kN mm)	Incr. of energy (%)
1	A-FP/f0-0	0	2.37	22.84	9.64	–	2147.5	–
2	A-FP/f0-5	0.4	2.53	28.75	11.36	18	2680.9	25
3	A-FP/F1-0	0.8	2.67	37.30	13.97	45	3808.3	78
4	A-FP/F1-5	1.2	2.63	42.50	16.16	68	4037.6	88
5	A-FPhf/f1-0	0.8	2.20	25.90	11.77	22	2996.3	40
6	A-FPhf/f1-5	1.2	2.11	27.10	12.84	33	3228.5	50
7	A-FPhs/f1-0	0.8	2.48	24.40	9.85	2	2524.7	18
8	A-FPhs/f1-5	1.2	2.58	27.40	10.62	10	2678.7	25
1	A-PP/f0-0	0	2.33	24.85	10.60	0	2122	0
2	A-PP/F1-0	0.8	2.48	33.60	13.55	28	2838	34
3	A-PP/F1-5	1.2	2.40	35.40	14.75	39	3237	53
4	A-PPhf/f1-0	0.8	2.21	27.55	12.47	18	2452	16
5	A-PPhf/f1-5	1.2	2.13	28.80	13.52	28	2732	29
6	A-PPhs/f1-0	0.8	2.23	25.80	11.57	9	2206	4
7	A-PPhs/f1-5	1.2	1.90	22.30	11.75	11	2226	5

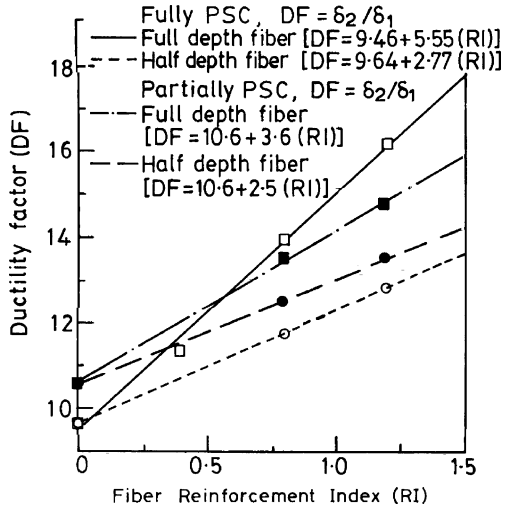

Fig. 9. Variation of ductility factor (DF) with fiber-reinforcement index (RI).

The ductility factor was found to increase with fiber inclusion (Fig. 9). In the case of fully prestressed beams specimens, the increase of ductility factor due to fiber addition was found to be more for the beams having full depth fiber (Table 4). These values were lesser for the beams having fibers over half depth over full length of the beam and half depth over shear span only and these have also been tabulated in Table 4. In the case of partially prestressed beam, ductility factor (Table 4) due to fiber content was more in prestressed concrete beams with full depth fiber as compared to the corresponding prestressed concrete beams with half depth fiber. The variation of ductility factor with the addition of fiber has been represented in Fig. 9 and it can be modelled using regression analysis as:

$$\mathrm{DF} = A + B(\mathrm{RI}) \tag{43}$$

where A and B are the correlation coefficients which are as shown in Fig. 9.

The energy absorbed was calculated by measuring the area under the load–deflection curves up to 2Δ, where Δ was the deflection at peak load. The value of 2Δ was selected on the basis of the information being the limiting value available from the test results. The energy absorbed for all 15 beams has been given in Table 4. Fig. 10 shows the variation of energy absorption with RI. From Table 4 and Fig. 10 it is seen that, there is a significant increase in energy absorbed with the inclusion of fibers. The energy absorption values were slightly lower for the half depth fiber reinforced prestressed concrete

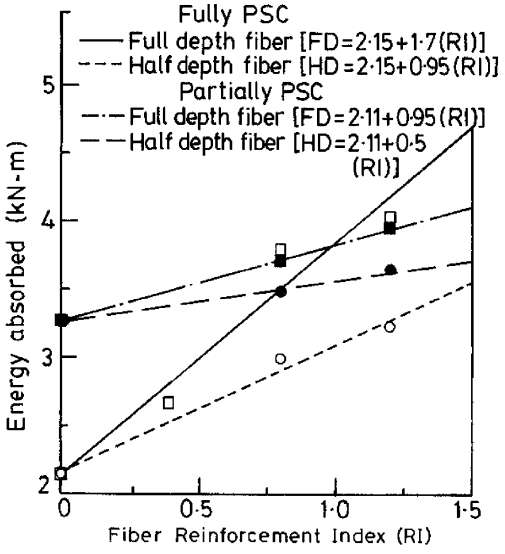

Fig. 10. Variation of energy absorbed with fiber-reinforcement index (RI).

beams as compared to the full depth fiber-reinforced concrete prestressed beams.

The strength capacity enhancement for beams having fibers has been provided in Table 1. The load carrying capacity is as much as 20% more for beams with 1.5% fiber by volume of concrete over the full beam (A-FP/F1-5) than for the corresponding plain concrete beam (control beam). Table 4 highlights a ductility factor enhancement of 68% for the same beam. Clearly mixing 1.5% by volume of concrete of fiber into the mix will not reduce the speed of construction as it is only another additive in the mix. However, this would result in tremendous performance enhancement or a corresponding reduction in cross-section (material savings) of the beam for a desired performance making it economical.

If only partial depth fiber is provided as an alternative (A-FPhf/F1-5 1.5% fiber by volume of concrete over half the beam depth), the need to have two mixes appears feasible only in a controlled set-up such as a precast concrete plant, where economy of scale will play a role, or at sites where adequate care is taken during construction. This may in turn slow down the speed of construction. The strength enhancement for this beam is 14% in terms of load and 33% in terms of ductility (Table 4). From the test results it is seen that partial depth fibers are quite adequate in providing similar structural capacity as the corresponding beam with fiber over the full depth. However, the ductility of such members is lower, as discussed, limiting the application of this technology to elements unlikely to be exposed to fatigue loads. The possibility of mass producing members, e.g., precast elements, or special long span girder elements, suggests that considerable economy would be achieved through reduced use of fibers (partial depth fibers) in these members. Material savings is evident from the above in terms of reduced cross-section for equivalent structural performance as a plain concrete beam. If unit costs of a cubic meter of concrete and the cost of steel fiber is also considered, it is clear that improved performance of the beam with fiber pays itself off in terms of an improved performance over the same or longer term.

Finally, while only one beam of each type was employed in the series of beams studied, the trends observed were consistent across the full series of beams—fully and partially prestressed beams with full or partial depth fiber, validating the conclusions reported in this study in a general sense. The specific percentage gains indicated should be taken only as an indicator.

5. Conclusions

Based on the experimental results and analytical predictions for eight fully and seven partially prestressed SFRC beam specimens the following conclusions were drawn in the present study.

1. The addition of fibers to the fully/partially prestressed beams was found to enhance both the cracking and ultimate flexural strength of the beams. The presence of trough shape fiber in HSC changes the basic characteristics of the load–deflection curve. The ascending portion of the load–deflection changes very slightly, but the descending portion becomes less steep, which resulted in a higher ductility and toughness of the material. At a particular load level the various deformational characteristics viz., deflection, strain in the prestressing wire and deformed bar, and curvature were reduced due to an increase in the fiber content as compared to plain concrete prestressed beams at the corresponding stages of loading.

2. Inclusion of fibers in half the depth in the shear span alone resulted in little increase in the ultimate load and deformational characteristics when compared to plain concrete beams. This type of inclusion is therefore not recommended.

3. When compared to fully prestressed beams, earlier initial cracks were observed in the partially prestressed beams. The ultimate load carrying capacity of these beams was less compared to the corresponding fully prestressed beams. The deflection at a particular load level was found to be more as compared the corresponding fully prestressed beams. The maximum increase in flexural strength in fully prestressed beams due to addition of fibers was 8%, 16%, and 21% for the fiber volume fraction of 0.5%, 1.0%, and 1.5%, respectively. All the prestressed beams failed in flexure mode accompanied by fiber pull-out across the cracks rather than by fiber fracture.

4. The toughness and ductility of the prestressed HSC beams increased with an increase in the fiber content. The ductility ratio is greater for full depth fiber-reinforced concrete beams compared to partial depth fiber-reinforced beams. Addition of fiber increased both the ductility and energy absorption capacity. The maximum increase in ductility was 18%, 45%, and 68%, and percentage increase in energy absorption was 25%, 78% and 88% for the fully prestressed beams with full depth fiber v_f of 0.5%, 1.0%, and 1.5%, respectively. In the case of partially prestressed beams, the percentage increase in ductility due to addition of fibers was found to be 28% and 39% with increase in energy absorption of 34% and 53% for the beam with v_f 1.0% and 1.5%, respectively. In the case of fully prestressed beam having partial depth FRC over full length, the increase in ductility was 22% and 33% with percentage increase in energy absorption of 40% and 50% for the beam with v_f 1.0% and 1.5%, respectively. However, a percentage increase in ductility factor of 18% and 28% with increase in energy absorption of 16% and 29% was seen in the case of partially prestressed beam having partial fiber depth.

5. Inclusion of fibers over a partial depth in the tensile side of the prestressed flexural structural members would be economical and lead to considerable cost saving in the design without sacrificing the desired performance in the area of building elements. Full depth fiber-reinforced members will be necessary in some special structures subject to large strain rates of loading and fatigue.

6. The proposed analytical expressions using model 1 and 2, for moment–curvature relationship, load–deflection response provides good comparison between predicted and experimental results for high-strength prestressed concrete beams containing trough shape fibers. As compared to model 1, model 2 predicts the performance better in terms of ultimate load, moment and postpeak ductility.

References

[1] Ghalib MA. Moment capacity of steel fiber-reinforced small concrete slabs. ACI J. Proceedings, vol. 77. 1980. p. 247–57.
[2] Gunashekaran M. The strength and behavior of light weight concrete beams made with fly-ash aggregates and fiber-reinforced partially. Indian Concr J 1975;49(11):332–4.
[3] Hannant DJ. Fiber cements and fiber concretes. NY: John Wiley and Sons; 1978. p. 35–40.
[4] Hassoun MN. Ultimate strength of reinforced light weight fibrous concrete beams. In: Swamy RN, Barr B, editors. Fiber reinforced cements and concretes, recent developments. Elsevier Science Publishers Ltd; 1989. p. 467–78.
[5] Henager CH, Doherty TJ. Analysis of reinforced fibrous concrete beams. Proc ASCE 1976;102(ST1):177–88.
[6] Henager CH. Ultimate strength of reinforced steel fibrous concrete beams. Fiber reinforced materials: design and engineering applications, Proceedings of the Conference, London, 1977. p. 165–73.
[7] Hughes BP. Experimental test result for flexure and direct tension of fiber cement composites. Int J Cement Compos Lightweight Concr 1981;3(1):13–8.
[8] IS: 269-1976. Specifications for ordinary and low heat port-land cement (third revision). Indian Standards Institution, New Delhi.
[9] IS: 383-1970. Specifications for coarse and fine aggregate from natural sources for concrete (second revision). Indian Standard Institution, New Delhi.
[10] Nagaraj TS, Banu Z. Generalization of Abram's law. Cement Concr Res 1996;26(6):933–42.
[11] Padmarajaiah SK. Influence of fibers on the behavior of high strength concrete in fully/partially prestressed beams: an experimental and analytical study. Ph.D. thesis. Indian Institute of Science, submitted.
[12] Padmarajaiah SK, Ramaswamy A. Comparative flexural response of full and partial depth fibrous high strength concrete prisms containing trough shape steel fibers. J Mater Eng, ASCE 2002;14(2):130–6.
[13] Padmarajaiah SK, Ramaswamy A. Crack width predictions for high strength concrete fully/partially prestressed beam specimens containing steel fibers. Struct J, ACI 2001:852–61.
[14] Rahimi MM, Kelser CE. Partially steel-fiber reinforced mortar. J Struct Division, ASCE 1979;105(ST1):101–9.
[15] Ramzi B, Abdullah A, Aziz OQ. Flexural strength of reinforced concrete T-beams with steel fibers. Cement Concr Compos 1999;21(2):263–8.
[16] Ravindrarajah RS, Tam ST. Flexural strength of steel fiber reinforced concrete beams. Int J Cement Compos Lightweight Concr 1984;6(4):273–8.
[17] Romualdi JP, Mandel JA. Tensile strength of concrete affected by uniformly distributed and closely spaced short lengths of wire reinforcement. ACI J 1964;61(6):657–70.
[18] Soroushian P, Lee CD. Distribution and orientation of fibers in steel fiber reinforced concrete. ACI Mater J 1990;87(5):433–9.
[19] SP-23, Hand Book on concrete mixes. Indian Standards Institution, New Delhi, 1982.
[20] Swamy RN, Mangat PS, Rao CVSK. The mechanics of fiber reinforcement of cement matrices, fiber reinforced concrete. SP-44, ACI, Detroit, 1974. p. 1–28.
[21] Swamy RN, Sa'ad A, Al-Ta'an. Deformation and ultimate strength in flexure of reinforced concrete beams made with steel fiber concrete. Proc ACI Jl 1981;78(5):395–405.
[22] Swamy RN, Mangat PS. The interfacial bond stress in steel fiber cement composites. Cement Concr Res 1975;6(5):641–50.
[23] IS-1343. Code of practice for Prestressed Concrete (First Revision). Indian Standards Institute, New Delhi, 1980.